JOURNAL OF COMPUTATIONAL PHYSICS 109, 76-83 (1993)

Cylindrical Smoothed Particle Hydrodynamics

A. G. PETSCHEK

Department of Physics, New Mexico Institute of Mining and Technology, Socorro, New Mexico 87081

AND

L. D. LIBERSKY

Center for Explosives Technology Research, New Mexico Institute of Mining and Technology, Socorro, New Mexico 87801 and Space Kinetic Impact and Debris Branch, Phillips Laboratory, Kirtland, New Mexico 87117

Received December 11, 1991; revised March 11, 1993

Smoothed particle hydrodynamics (SPH) is formulated in two-dimensional axisymmetric coordinates. Starting with a three-dimensional Cartesian representation of SPH we integrate out the angular component and find a two-dimensional cylindrical description. A smoothed "particle" in this formulation becomes a smoothed "torus." The hoop stress, resulting from interactions within the toroidal ring, is a natural consequence of the derivation. No pathological behavior is observed at the symmetry axis. The formulation has been extended to include the entire stress tensor, not just the pressure, and is therefore applicable to a wide range of materials and flow speeds. Three calculations are presented and compared to known results. © 1993 Academic Press, Inc.

INTRODUCTION

Smoothed particle hydrodynamics (SPH) is unique in computational continuum dynamics in that it uses no spatial mesh. It is a pure Lagrangian particle method developed by Lucy [1], Monaghan [2–4], Gingold [5, 6], and Benz [7]. SPH has many nice features such as robustness, conceptual simplicity, ease of adding new physics, a natural treatment of voids, and the ability to handle large strains in a Lagrangian frame. The method has been used almost exclusively for astrophysical applications where the flows are three-dimensional (3D), involve fluids, and are often self-gravitating. The relative ease of doing 3D calculations with SPH is demonstrated by the abundance of such simulations appearing in the astrophysical literature. One reason why 3D calculations are more easily done with SPH than other techniques is the conceptual simplicity of the method, but it also appears that SPH has an efficiency advantage over Eulerian in 3D [8], at least for some problems. Recently, Libersky and Petschek [9] have incorporated material strength and the complete stress and strain tensors into Cartesian formulations of SPH using linear elasticity. Although no direct comparisons with Eulerian codes have been made for problems similar to those reported there, in many cases we see little evidence for the efficiency gains reported in [8]. Although many three-dimensional SPH calculations can be performed on workstations, the run times are still significant and there is a strong need for a two-dimensional axisymmetric formulation of smoothed particle hydrodynamics.

Some axisymmetric SPH algorithms have been formulated and are currently in use. Stellingwerf [10] simply multiplies the ordinary Cartesian interpolational kernel (smoothing function) by $1/r$ and renormalizes. Coleman and Bicknell [11] proceed in a similar way. These approaches are attractive in their simplicity and seem to perform well for many hydrodynamic flows. But, the hoop stress, which one expects to see in cylindrical coordinates (see Fig. 1 and discussion below Eq. (25)) appears to be absent.

The companion paper "High Strain Lagrangian Hydrodynamics" appearing in this volume contains material relevant to this paper. In order to avoid repetition we simply refer the reader to "HSLH."

THE MOMENTUM EQUATION: KERNEL ESTIMATES AND COORDINATE FRAMES

The acceleration of a Lagrangian volume element subject to elastic forces is

$$\frac{dU^\alpha}{dt} = -\frac{1}{\rho}\frac{\partial \sigma^{\alpha\beta}}{\partial x^\beta}. \tag{1}$$

0021-9991/93 $5.00

Copyright © 1993 by Academic Press, Inc.
All rights of reproduction in any form reserved.

Dependent variables are the density ρ, velocity vector U^α, and the stress tensor $\sigma^{\alpha\beta}$. Independent variables are the spatial coordinates x^β and the time t. The time derivative is a total (Lagrangian) derivative. We will use both tensor (superscripted) and vector (bold) notation in the derivations. It is convenient in deriving SPH equations to rewrite (1) as a total derivative and a correction,

$$\frac{dU^\alpha}{dt} = -\frac{\partial}{\partial x^\beta}\left(\frac{\sigma^{\alpha\beta}}{\rho}\right) - \frac{\sigma^{\alpha\beta}}{\rho^2}\frac{\partial \rho}{\partial x^\beta}. \tag{2}$$

This will lead to forces between particles with manifest Galilean invariance and action equal to reaction (Eq. (6), below). We seek an estimate of the acceleration at a point $(\mathbf{x})$ using nearby information and therefore multiply by an interpolating kernel (W) and integrate over all space:

$$\left\langle \frac{dU^\alpha(\mathbf{x})}{dt} \right\rangle = \int W(\mathbf{x}-\mathbf{x}')\frac{dU^\alpha(\mathbf{x}')}{dt}\,d\mathbf{x}' \tag{3}$$

$$\left\langle \frac{dU^\alpha(\mathbf{x})}{dt} \right\rangle = -\int W \frac{\partial}{\partial x'^\beta}\left(\frac{\sigma^{\alpha\beta}(\mathbf{x}')}{\rho(\mathbf{x}')}\right) d\mathbf{x}' - \int W \frac{\sigma^{\alpha\beta}(\mathbf{x}')}{\rho^2(\mathbf{x}')}\frac{\partial \rho(\mathbf{x}')}{\partial x'^\beta}\,d\mathbf{x}'. \tag{4}$$

If the last term in (4) is linearized, then after an integration by parts we can write the kernel estimate of the acceleration as

$$\left\langle \frac{dU^\alpha(\mathbf{x})}{dt} \right\rangle = -\frac{\partial}{\partial x^\beta}\int W \frac{\sigma^{\alpha\beta}(\mathbf{x}')}{\rho(\mathbf{x}')}\,d\mathbf{x}' - \frac{\sigma^{\alpha\beta}(\mathbf{x})}{\rho^2(\mathbf{x})}\frac{\partial}{\partial x^\beta}\int W\rho(\mathbf{x}')\,d\mathbf{x}'. \tag{5}$$

If nearby information is available only at discrete points j, the volume element is replaced by m_j/ρ_j and the integrals by summations [7] giving

$$\frac{dU_i^\alpha}{dt} = \left\langle \frac{dU^\alpha(\mathbf{x}_i)}{dt} \right\rangle = -\frac{\partial}{\partial x_i^\beta}\sum_j m_j \frac{\sigma_j^{\alpha\beta}}{\rho_j^2} W_{ij} - \frac{\sigma_i^{\alpha\beta}}{\rho_i^2}\frac{\partial}{\partial x_i^\beta}\sum_j m_j W_{ij}. \tag{6}$$

This equation, in which only $W_{ij} = W(\mathbf{x}_i - \mathbf{x}_j)$ depends on the continuous variable x_i, gives the acceleration of a fluid particle i due to forces from neighboring particles j.

Let us write out the x and z components of (6) in a three-dimensional Cartesian frame of reference,

$$\begin{aligned}\frac{dU_i^x}{dt} = &-\frac{\partial}{\partial x_i}\sum_j m_j \frac{\sigma_j^{xx}}{\rho_j^2} W_{ij} - \frac{\partial}{\partial y_i}\sum_j m_j \frac{\sigma_j^{xy}}{\rho_j^2} W_{ij} \\ &-\frac{\partial}{\partial z_i}\sum_j m_j \frac{\sigma_j^{xz}}{\rho_j^2} W_{ij} - \frac{\sigma_i^{xx}}{\rho_i^2}\frac{\partial}{\partial x_i}\sum_j m_j W_{ij} \\ &-\frac{\sigma_i^{xy}}{\rho_i^2}\frac{\partial}{\partial y_i}\sum_j m_j W_{ij} - \frac{\sigma_i^{xz}}{\rho_i^2}\frac{\partial}{\partial z_i}\sum_j m_j W_{ij}\end{aligned} \tag{7}$$

and

$$\begin{aligned}\frac{dU_i^z}{dt} = &-\frac{\partial}{\partial x_i}\sum_j m_j \frac{\sigma_j^{xz}}{\rho_j^2} W_{ij} - \frac{\partial}{\partial y_i}\sum_j m_j \frac{\sigma_j^{yz}}{\rho_j^2} W_{ij} \\ &-\frac{\partial}{\partial z_i}\sum_j m_j \frac{\sigma_j^{zz}}{\rho_j^2} W_{ij} - \frac{\sigma_i^{xz}}{\rho_i^2}\frac{\partial}{\partial x_i}\sum_j m_j W_{ij} \\ &-\frac{\sigma_i^{yz}}{\rho_i^2}\frac{\partial}{\partial y_i}\sum_j m_j W_{ij} - \frac{\sigma_i^{zz}}{\rho_i^2}\frac{\partial}{\partial z_i}\sum_j m_j W_{ij}.\end{aligned} \tag{8}$$

We now change the coordinate frame from 3D Cartesian to 3D cylindrical using the contravariant tensor transformation $\sigma^{\alpha\beta} = a_r^\alpha a_s^\beta \sigma^{rs}$, where a_r^α are the direction cosines. Finally, without loss of generality because of the cylindrical symmetry, we choose $\theta_i = 0$. This gives

$$\begin{aligned}\frac{dU_i^r}{dt} = &-\frac{\partial}{\partial r_i}\sum_j \frac{m_j}{\rho_j^2}(\sigma_j^{rr}\cos^2\theta_j + \sigma_j^{\theta\theta}\sin^2\theta_j) W_{ij} \\ &-\frac{1}{r_i}\frac{\partial}{\partial \theta_i}\sum_j \frac{m_j}{\rho_j^2}(\sigma_j^{rr} - \sigma_j^{\theta\theta})\cos\theta_j \sin\theta_j W_{ij} \\ &-\frac{\partial}{\partial z_i}\sum_j \frac{m_j}{\rho_j^2}\sigma_j^{rz}\cos\theta_j W_{ij} - \frac{1}{\rho_i^2}\sigma_i^{rr}\frac{\partial}{\partial r_i}\sum_j m_j W_{ij} \\ &-\frac{1}{\rho_i^2}\sigma_i^{rz}\frac{\partial}{\partial z_i}\sum_j m_j W_{ij}\end{aligned} \tag{9}$$

and

$$\begin{aligned}\frac{dU_i^z}{dt} = &-\frac{\partial}{\partial r_i}\sum_j \frac{m_j}{\rho_j^2}\sigma_j^{rz}\cos\theta_j W_{ij} - \frac{1}{r_i}\frac{\partial}{\partial \theta_i}\sum_j \frac{m_j}{\rho_j^2}\sigma_j^{rz}\sin\theta_j W_{ij} \\ &-\frac{\partial}{\partial z_i}\sum_j \frac{m_j}{\rho_j^2}\sigma_j^{zz} W_{ij} - \frac{1}{\rho_i^2}\sigma_i^{rz}\frac{\partial}{\partial r_i}\sum_j m_j W_{ij} \\ &-\frac{1}{\rho_i^2}\sigma_i^{zz}\frac{\partial}{\partial z_i}\sum_j m_j W_{ij}.\end{aligned} \tag{10}$$

Equations (9) and (10) determine the radial and axial acceleration of a particle in cylindrical coordinates in axisymmetric problems. By letting the number of particles in a ring approach infinity we can integrate out the angular components and obtain a two-dimensional formulation of SPH in cylindrical symmetry.

INTEGRATION

The summations in (9) and (10) represent sums over particles in a ring as well as sums over neighboring rings. We let the number of particles in a ring approach infinity so that an integration over the ring can be performed, at least for convenient kernels. The requisite integrations in (9) and (10) can be readily done with a Gaussian kernel, which, however, is computationally less efficient than the B-splines normally used in SPH. The Gaussian $\exp(-r^2/h^2)$ in two dimensions effectively averages over a range $H=h$, the root mean square expectation of r, but gives poor results if it is cut off at $r<3h$ [4], whereas the commonly used B-spline has compact support on $r<2h$ and $\langle r^2\rangle^{1/2}=H=0.80h$. Thus the Gaussian requires $(3H_B/2H_G)^2=1.5$ times as many neighbors to be handled for the same effective averaging as the B-spline. Run times go like the square of the cutoff distance over the square of the range making the Gaussian less efficient than the spline. We have not yet been able to extend our technique to B-splines. A Gaussian kernel has the following form in a three-dimensional cylindrical coordinate frame for a particle located at (r_i, θ_i, z_i).

$$W(x-x_i, h) = e^{-\{(r-r_i)^2+(z-z_i)^2+2rr_i[1-\cos(\theta-\theta_i)]\}/h^2} = Ge^{-\xi}e^{\xi\cos(\theta-\theta_i)}. \tag{11}$$

Since for a torus of mass m the mass in the interval $d\theta$ is $m\,d\theta/2\pi$, the θ integration of (11) gives the two-dimensional "cylindrical" kernel

$$W_c(\xi) = I_0(\xi)\,e^{-\xi}G, \tag{12}$$

where $\xi=2r_ir/h^2$, I_0 is the modified Bessel function of zero order, and G is the two-dimensional Gaussian function $\exp\{-[(r-r_i)^2+(z-z_i)^2]/h^2\}$. Other integrals required by (9) and (10) are

$$\frac{1}{2\pi}\int W\cos\theta\,d\theta = W_c\frac{I_1(\xi)}{I_0(\xi)}, \tag{13}$$

$$\frac{1}{2\pi}\int W\cos^2\theta\,d\theta = W_c\frac{I_0(\xi)+I_2(\xi)}{2I_0(\xi)}, \tag{14}$$

$$\frac{1}{2\pi}\int \frac{dW}{d\theta}\sin\theta\,d\theta = -\xi W_c\frac{I_0(\xi)-I_2(\xi)}{2I_0(\xi)}, \tag{15}$$

$$\frac{1}{2\pi}\int \frac{dW}{d\theta}\sin\theta\cos\theta\,d\theta = -\xi W_c\frac{I_1(\xi)-I_3(\xi)}{4I_0(\xi)}. \tag{16}$$

After the integrations have been performed on (9) and (10), the radial and axial accelerations of a particle are

$$\begin{aligned}\frac{dU_i^r}{dt} = &-\frac{\partial}{\partial r_i}\sum_j\frac{m_j}{\rho_j^2}\left(\sigma_j^{rr}\frac{I_0+I_2}{2I_0}+\sigma_j^{\theta\theta}\frac{I_0-I_2}{2I_0}\right)W_c\\ &-\frac{\partial}{\partial z_i}\sum_j\frac{m_j}{\rho_j^2}\sigma_j^{rz}\frac{I_1}{I_0}W_c\\ &-\frac{\sigma_i^{rr}}{\rho_i^2}\frac{\partial}{\partial r_i}\sum_j m_jW_c-\frac{\sigma_i^{rz}}{\rho_i^2}\frac{\partial}{\partial z_i}\sum_j m_jW_c\\ &-\frac{2}{h^2}\sum_j\frac{m_j}{\rho_j^2}r_j(\sigma_j^{rr}-\sigma_j^{\theta\theta})\left(\frac{I_1-I_3}{4I_0}\right)W_c\end{aligned} \tag{17}$$

$$\begin{aligned}\frac{dU_i^z}{dt} = &-\frac{\partial}{\partial r_i}\sum_j\frac{m_j}{\rho_j^2}\sigma_j^{rz}\frac{I_1}{I_0}W_c-\frac{2}{h^2}\sum_j\frac{m_j}{\rho_j^2}r_j\sigma_j^{rz}\frac{I_0-I_2}{2I_0}W_c\\ &-\frac{\partial}{\partial z_i}\sum_j\frac{m_j}{\rho_j^2}\sigma_j^{zz}W_c-\frac{\sigma_i^{rz}}{\rho_i^2}\frac{\partial}{\partial r_i}\sum_j m_jW_c\\ &-\frac{\sigma_i^{zz}}{\rho_i^2}\frac{\partial}{\partial z_i}\sum_j m_jW_c,\end{aligned} \tag{18}$$

where henceforth the argument of W_c and the Bessel functions is $\xi=2r_ir_j/h^2$.

DIFFERENTIATION

The final step in the derivation is differentiation. The derivatives required by (17) and (18) are

$$\frac{\partial W_c}{\partial r_i} = -\frac{2}{h^2}\left(r_i-r_j\frac{I_1}{I_0}\right)W_c \tag{19}$$

$$\frac{\partial W_c}{\partial z_i} = -\frac{2}{h^2}(z_i-z_j)\,W_c \tag{20}$$

$$\frac{\partial}{\partial r_i}\left(\frac{I_1}{I_0}W_c\right) = -\frac{2}{h^2}\left[r_i\frac{I_1}{I_0}-\frac{1}{2}r_j\left(1+\frac{I_2}{I_0}\right)\right]W_c \tag{21}$$

$$\frac{\partial}{\partial z_i}\left(\frac{I_1}{I_0}W_c\right) = -\frac{2}{h^2}(z_i-z_j)\frac{I_1}{I_0}W_c \tag{22}$$

$$\frac{\partial}{\partial r_i}\left(\frac{I_2}{I_0}W_c\right) = -\frac{2}{h^2}\left(r_i\frac{I_2}{I_0}-r_j\frac{I_1+I_3}{2I_0}\right)W_c. \tag{23}$$

The final form for the particle accelerations is obtained by using the derivatives (19)–(23) in (17, 18) and collecting terms:

$$\begin{aligned}\frac{dU_i^r}{dt} = &\frac{2}{h^2}\sum_j m_jW_c\left\{\frac{\sigma_j^{rr}}{\rho_j^2}\left[r_i\left(\frac{I_0+I_2}{2I_0}\right)-r_j\left(\frac{I_1}{I_0}\right)\right]\right.\\ &+\frac{\sigma_j^{\theta\theta}}{\rho_j^2}r_i\left(\frac{I_0-I_2}{2I_0}\right)+\frac{\sigma_j^{rz}}{\rho_j^2}(z_i-z_j)\frac{I_1}{I_0}\\ &\left.+\frac{\sigma_i^{rr}}{\rho_i^2}\left(r_i-r_j\frac{I_1}{I_0}\right)+\frac{\sigma_i^{rz}}{\rho_i^2}(z_i-z_j)\right\}\end{aligned} \tag{24}$$

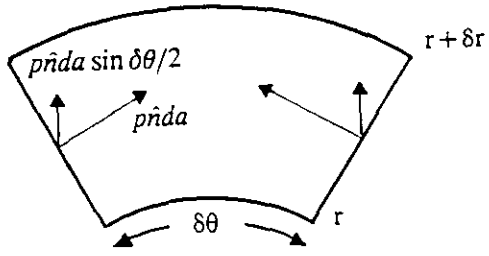

FIG. 1. Volume element of a hydrodynamic (no deviatoric stresses) problem, illustrating the outward force due to pressure forces on surfaces of constant θ. If the pressure is constant, this "hoop stress" gives zero net outward force as required when combined with the outward pressure force on the inner cylindrical surface at r and the greater inward force on the outer surface at $r+\delta r$.

$$\frac{dU_i^z}{dt}=\frac{2}{h^2}\sum_j m_j W_c\left\{\frac{\sigma_j^{rz}}{\rho_j^2}\left(r_i\frac{I_1}{I_0}-r_j\right)+\frac{\sigma_j^{zz}}{\rho_j^2}(z_i-z_j)\right.$$
$$\left.+\frac{\sigma_i^{rz}}{\rho_i^2}\left(r_i-r_j\frac{I_1}{I_0}\right)+\frac{\sigma_i^{zz}}{\rho_i^2}(z_i-z_j)\right\}. \tag{25}$$

Equations (24) and (25) give the radial and axial accelerations of a smoothed particle (torus) for cylindrically symmetric problems. The form of these equations, including the Bessel functions, is due to the choice of kernel (Gaussian). An important consequence of the derivation is that if $i=j$ in the summations above, the right-hand sides no longer vanish as they do in Cartesian formulations. This contribution to the acceleration is a "self-force" due to particle interactions within a toroidal ring and represents the hoop stress tending to push material away from the axis. In continuum formulations it is produced by the outward component of the stress exerted across the surfaces of constant θ bounding the volume element, as in Fig. 1.

THE ENERGY EQUATION

The equation for the specific internal energy is

$$\frac{dE}{dt}=-\frac{\sigma^{\alpha\beta}}{\rho}\frac{\partial U^\alpha}{\partial x^\beta}. \tag{26}$$

As with the momentum equation, we write (26)

$$\frac{dE}{dt}=-\frac{\sigma^{\alpha\beta}}{\rho^2}\frac{\partial \rho U^\alpha}{\partial x^\beta}+\frac{\sigma^{\alpha\beta}U^\alpha}{\rho^2}\frac{\partial\rho}{\partial x^\beta}. \tag{27}$$

Proceeding as before, (27) is transformed into a particle equation. The result is

$$\frac{dE_i}{dt}=\frac{\sigma_i^{\alpha\beta}}{\rho_i^2}\frac{\partial}{\partial x_i^\beta}\sum_j (U_i^\alpha-U_j^\alpha)\,m_j W_{ij}, \tag{28}$$

where the reformulation of (26) into (27) has led to the appearance of the velocity difference, and therefore Galilean invariance. Expanding (28) into Cartesian three-space gives

$$\frac{dE_i}{dt}=\frac{\sigma_i^{xx}}{\rho_i^2}\frac{\partial}{\partial x_i}\sum_j (U_i^x-U_j^x)\,m_j W_{ij}$$
$$+\frac{\sigma_i^{xy}}{\rho_i^2}\frac{\partial}{\partial y_i}\sum_j (U_i^x-U_j^x)\,m_j W_{ij}$$
$$+\frac{\sigma_i^{xz}}{\rho_i^2}\frac{\partial}{\partial z_i}\sum_j (U_i^x-U_j^x)\,m_j W_{ij}$$
$$+\frac{\sigma_i^{yx}}{\rho_i^2}\frac{\partial}{\partial x_i}\sum_j (U_i^y-U_j^y)\,m_j W_{ij}$$
$$+\frac{\sigma_i^{yy}}{\rho_i^2}\frac{\partial}{\partial y_i}\sum_j (U_i^y-U_j^y)\,m_j W_{ij}$$
$$+\frac{\sigma_i^{yz}}{\rho_i^2}\frac{\partial}{\partial z_i}\sum_j (U_i^y-U_j^y)\,m_j W_{ij}$$
$$+\frac{\sigma_i^{zx}}{\rho_i^2}\frac{\partial}{\partial x_i}\sum_j (U_i^z-U_j^z)\,m_j W_{ij}$$
$$+\frac{\sigma_i^{zy}}{\rho_i^2}\frac{\partial}{\partial y_i}\sum_j (U_i^z-U_j^z)\,m_j W_{ij}$$
$$+\frac{\sigma_i^{zz}}{\rho_i^2}\frac{\partial}{\partial z_i}\sum_j (U_i^z-U_j^z)\,m_j W_{ij}. \tag{29}$$

Transformation of (29) into the $r-z$ plane of cylindrical three-space and choosing $\theta_i=0$ gives

$$\frac{dE_i}{dt}=\frac{\sigma_i^{rr}}{\rho_i^2}\frac{\partial}{\partial r_i}\sum_j (U_i^r-U_j^r\cos\theta)\,m_j W_{ij}$$
$$+\frac{\sigma_i^{rz}}{\rho_i^2}\frac{\partial}{\partial z_i}\sum_j (U_i^r-U_j^r\cos\theta)\,m_j W_{ij}$$
$$+\frac{\sigma_i^{rz}}{\rho_i^2}\frac{\partial}{\partial r_i}\sum_j (U_i^z-U_j^z)\,m_j W_{ij}$$
$$+\frac{\sigma_i^{zz}}{\rho_i^2}\frac{\partial}{\partial z_i}\sum_j (U_i^z-U_j^z)\,m_j W_{ij}$$
$$+\frac{\sigma_i^{\theta\theta}}{\rho_i^2}\frac{1}{r_i}\frac{\partial}{\partial\theta_i}\sum_j (U_i^z-U_j^z)\,m_j W_{ij}. \tag{30}$$

The θ-integration of (30) gives

$$\frac{dE_i}{dt}=\frac{\sigma_i^{rr}}{\rho_i^2}\frac{\partial}{\partial r_i}\sum_j\left(U_i^r-U_j^r\frac{I_1}{I_0}\right)m_jW_c+\frac{\sigma_i^{rz}}{\rho_i^2}\frac{\partial}{\partial z_i}\sum_j\left(U_i^r-U_j^r\frac{I_1}{I_0}\right)m_jW_{ij}+\frac{\sigma_i^{rz}}{\rho_i^2}\frac{\partial}{\partial r_i}\sum_j(U_i^z-U_j^z)\,m_jW_c+\frac{\sigma_i^{zz}}{\rho_i^2}\frac{\partial}{\partial z_i}\sum_j(U_i^z-U_j^z)\,m_jW_c+\frac{\sigma_i^{\theta\theta}}{\rho_i^2}\frac{1}{r_i}\frac{2}{h^2}\sum_j U_j^r\frac{I_0-I_2}{2I_0}m_jW_c. \tag{31}$$

Differentiation of (31) with the use of (19)–(23) gives the final form of the particle energy equation,

$$\frac{dE_i}{dt}=-\frac{2}{h^2}\sum_j m_jW_c\left\{\frac{\sigma_i^{rr}}{\rho_i^2}\left[U_i^r\left(r_i-r_j\frac{I_1}{I_0}\right)-U_j^r\left(r_i\frac{I_1}{I_0}-\frac{1}{2}r_j\left(1+\frac{I_2}{I_0}\right)\right)\right]+\frac{\sigma_i^{rz}}{\rho_i^2}\left[U_i^r(z_i-z_j)-U_j^r(z_i-z_j)\frac{I_1}{I_0}+(U_i^z-U_j^z)\left(r_i-r_j\frac{I_1}{I_0}\right)\right]+\left[\frac{\sigma_i^{zz}}{\rho_i^2}(U_i^z-U_j^z)(z_i-z_j)+\frac{\sigma_i^{\theta\theta}}{\rho_i^2}U_j^rr_j\frac{I_0-I_2}{2I_0}\right]\right\}. \tag{32}$$

CONSTITUTIVE EQUATIONS

The density equation and constitutive relations are treated as in "HSLH." We present here only the particle equations for the strain rates in 2D cylindrical coordinates. These equations are derived in the same way as the momentum and energy equations. The results are

$$\dot\varepsilon_i^{rr}=\frac{2}{h^2}\sum_j\frac{m_j}{\rho_j}W_c\left\{U_i^r\left(r_i-r_j\frac{I_1}{I_0}\right)-U_j^r\left[r_i\frac{I_1}{I_0}-\frac{1}{2}r_j\left(1+\frac{I_2}{I_0}\right)\right]\right\} \tag{33}$$

$$\dot\varepsilon_i^{zz}=\frac{2}{h^2}\sum_j\frac{m_j}{\rho_j}W_c(U_i^z-U_j^z)(z_i-z_j) \tag{34}$$

$$\dot\varepsilon_i^{\theta\theta}=\frac{2}{h^2}\sum_j\frac{m_j}{\rho_j}W_cr_jU_j^r\left(\frac{I_0-I_2}{2I_0}\right) \tag{35}$$

$$\dot\varepsilon^{rz}=-\frac{1}{h^2}\sum_j\frac{m_j}{\rho_j}W_c\left\{\left[U_j^r(z_i-z_j)\frac{I_1}{I_0}-U_i^r(z_i-z_j)\right]+\left[(U_j^z-U_i^z)\left(r_i-r_j\frac{I_1}{I_0}\right)\right]\right\}. \tag{36}$$

ARTIFICIAL VISCOSITY AND HEAT FLUX

For a discussion of artificial viscosity and artificial heat conduction we also refer the reader to "HSLH." We present here only the transformation of the μ_{ij} term ("HSLH," Eq. (26)) into cylindrical two-space. In order to obtain a form of $(\mathbf{U}_i-\mathbf{U}_j)\cdot(\mathbf{x}_i-\mathbf{x}_j)$ appropriate in axisymmetric coordinates we write it in cylindrical three-space, assuming $\theta_i=0$,

$$(\dot{\mathbf{x}}_i-\dot{\mathbf{x}}_j)\cdot(\mathbf{x}_i-\mathbf{x}_j)=r_{ij}\dot r_{ij}+(r_i\dot r_j+r_j\dot r_i)(1-\cos\theta_j)+z_{ij}\dot z_{ij}, \tag{37}$$

where

$$r_{ij}=r_i-r_j,\qquad z_{ij}=z_i-z_j. \tag{38}$$

We weight the artificial viscous interaction between particles i and j by the smoothing function (11) and integrate out the θ component. The result is

$$(\dot{\mathbf{x}}_i-\dot{\mathbf{x}}_j)\cdot(\mathbf{x}_i-\mathbf{x}_j)=\left[r_{ij}\dot r_{ij}+z_{ij}\dot z_{ij}+(r_i\dot r_j+\dot r_ir_j)\left(1-\frac{I_1}{I_0}\right)\right]W_c. \tag{39}$$

"HSLH" equations (25)–(27) with (39) for the dot product in "HSLH" equation (26) give the artificial viscosity used in our formulation of cylindrical SPH. Concerning the artificial heat flux, the transformation of "HSLH" equation (28) to cylindrical coordinates is trivial because differentiation of the three-dimensional Gaussian kernel gives $-2W_cx_{ij}/h^2$ so that "HSLH" equation (28) may be written as

$$H_i=-\frac{2}{h^2}\sum_j\frac{\zeta_{ij}}{\bar\rho_{ij}}(E_i-E_j)\,W_{ij}, \tag{40}$$

after which integration just replaces W_{ij} by W_c.

CALCULATIONS

The Noh Problem

Details of the Noh [12] problem are discussed in "HSLH." The calculations described here are the cylindrical Noh problem computed with our 1D cylindrical code and the spherical Noh problem computed with the 2D cylindrical code. Results of the 1D calculations are to be compared with the 2D Cartesian calculations in "HSLH." Results of the 2D calculations are to be compared with the 3D Cartesian run in "HLSH."

Figure 2a shows density profiles at $t=60$ obtained from 1D calculations using four different values of the smoothing length ($h=2.00$, 1.00, 0.50, 0.25) and two particles per h.

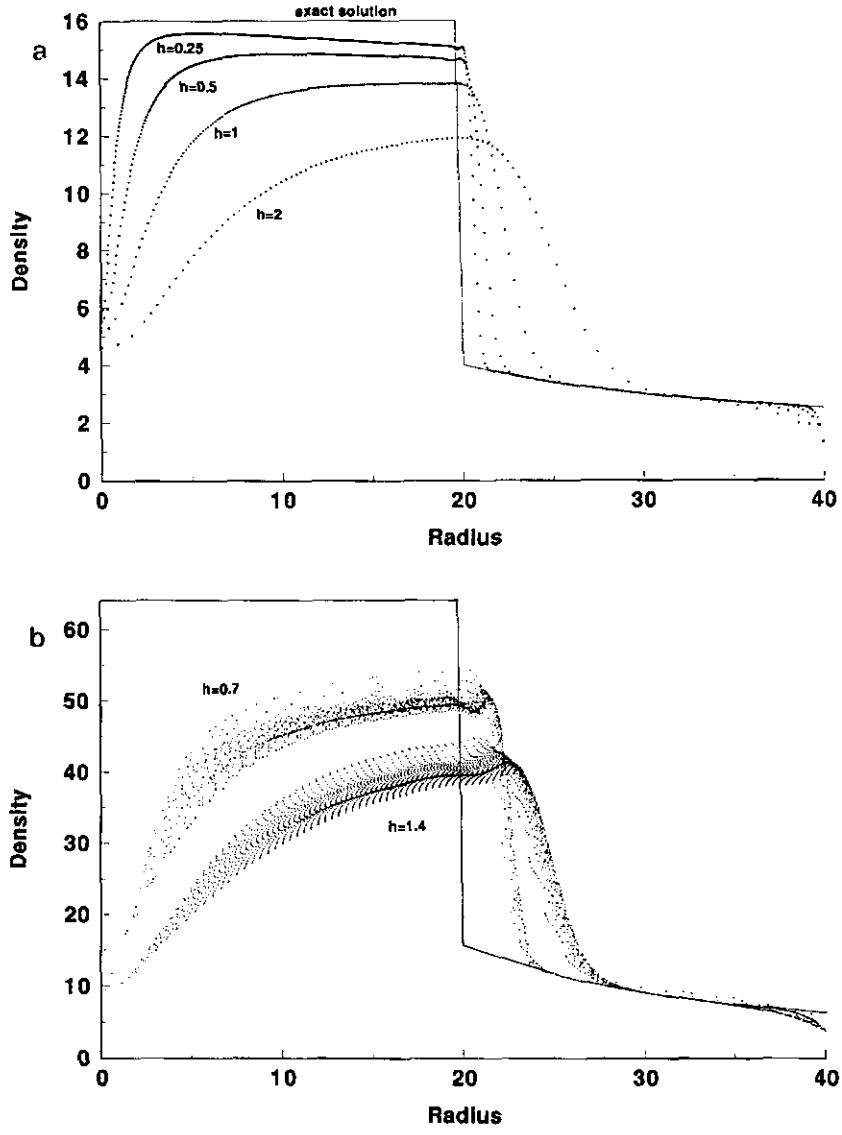

FIG. 2. (a) Density profiles at $t = 60$ for the cylindrical Noh implosion problem as computed with 1D cylindrical SPH. Results of four calculations, corresponding to different values of the smoothing length, and the exact solution are shown. (b) Density profiles at $t = 60$ for the spherical Noh implosion problem as computed with 2D cylindrical SPH. Results off two calculations, corresponding to different values of the smoothing length, and the exact solution are shown.

The density behind the shock is seen to be converging to the known solution $\rho = 16$. The artificial viscosity parameters had values $\alpha = \beta = 2.5$ in the calculations. No artificial heat flux was used ($g_1 = g_2 = 0$), hence the "hole" near the origin due to the "wall heating" effect. This "cylindrical" Noh problem can also be computed in 2D Cartesian coordinates. Results of those calculations are reported in "HSLH."

Figure 2b shows density profiles at $t = 60$ obtained from 2D calculations using two different values of the smoothing length ($h = 1.40$, 0.70) and one particle per h in each coordinate direction. There were 7904 and 31,576 particles used in the two calculations. As in the 1D case, the initial radius of the particle cloud was 100 with each particle given unit density, unit speed inward, and zero internal energy. We observe a "fuzzy" curve showing that symmetry has been lost in the calculation. The particles causing the problem are located near the axis of symmetry. We have not yet been able to identify the source of the error. In most calculations this behavior is not noticeable, but the severity of the spherical Noh implosion problem clearly manifests the error. The SPH solution falls short of the correct value of 64 for the density behind the shock front, although convergence with finer resolution is suggested in the figures. Crowley [13] has suggested that a tensor artificial viscosity, rather than the

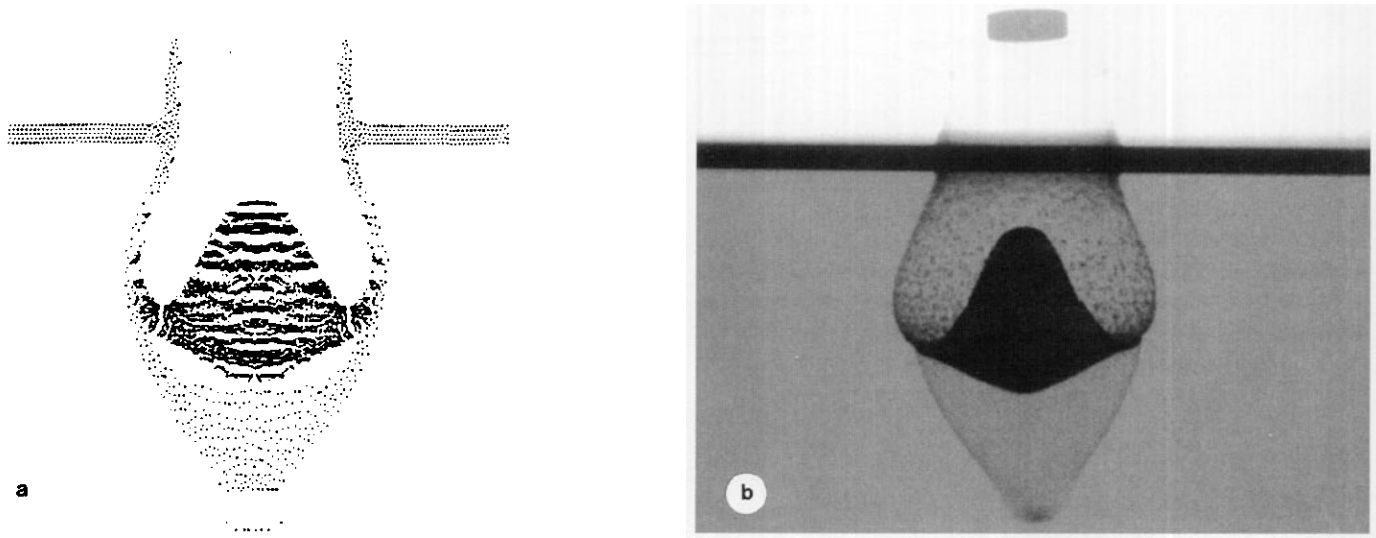

FIG. 3. Debris cloud at 6.4 μs for the impact of a copper pellet on an aluminum bumper plate at 5.55 km/s: (a) calculation; (b) experiment [14].

scalar formulation used here, would improve the solution. The 2D calculations took 3.5 and 23 h, respectively, on a 15 Mflop workstation.

Hypervelocity Impact

Figure 3a shows the SPH calculated debris cloud at 6.4 μs resulting from the normal impact of a 3-g copper disk (11.18 mm diameter, 3.45 mm thick) on a 2.87-mm thick aluminum bumber plate at 5.55 km/s. Figure 3b is a radiograph of the actual cloud 6.4 μs after impact [14]. The figures are scaled equally. The experimental impact was not exactly normal, the copper disk having a 5.4° yaw. Material properties used are given in Table I, where μ is the shear modulus, Y_0 is the yield strength, Γ is the Gruneisen coefficient, and (C, S) are the parameters in the linear shock velocity–particle velocity fit. We took the smoothing length to be $h = 0.16$ mm with 1.8 particles per h giving 15,564 particles total in the calculation. The calculation took 1175 cycles and 2.5 h on a 15 Mflop workstation. The peculiar shape of the aluminum debris cloud and copper disk are captured nicely by the simulation. Since the figures are scaled equally a ruler can be used to compare various dimensions in the SPH particle plot with the X-ray photograph. Such measurements show superb agreement between experiment and calculation.

Long Rod Penetration

Figure 4a shows the hole made by a tungsten rod penetrating a thick slab of steel as computed with SPH. The actual hole, as reported by Hohler and Stilp [15], is shown in Fig. 4b. The initial length and diameter of the tungsten rod were 29.12 mm and 2.80 mm, respectively ($L/D = 10.40$) and its speed was 3.58 km/s. Material properties used are given in Table I. The smoothing length used was $h = 0.47$ mm with two particles per h giving 51,238 paticles total. The calculation was run to 50 μs, at which time the hole growth ceased. This required 1493 cycles and 44 h on

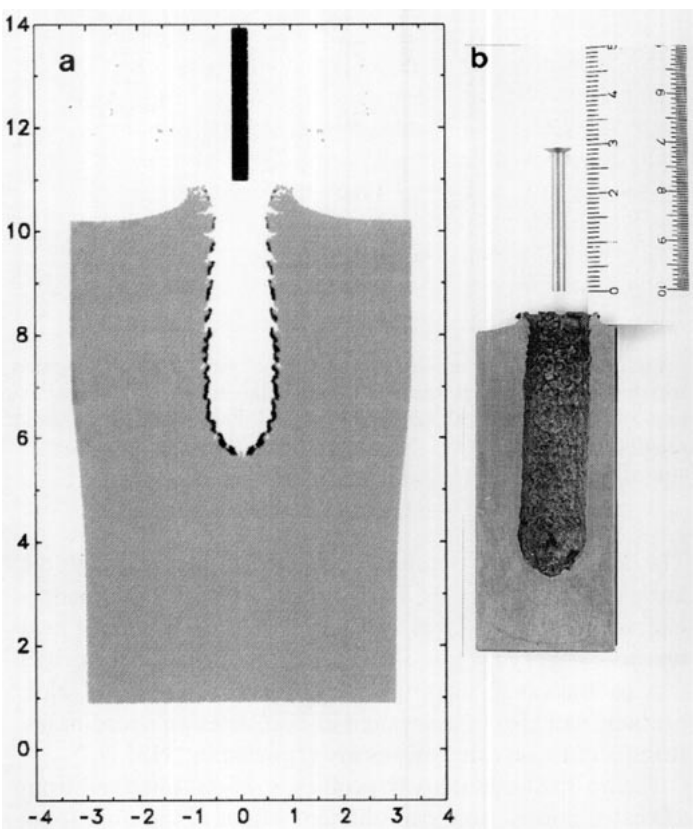

FIG. 4. Hole produced by the impact and penetration of a Tungsten rod ($L/D = 10.4$) into steel at 3.58 km/s: (a) calculation; (b) experiment [15].

TABLE I

Properties of Materials Used in the Calculations

	ρ_0 (g/cc)	C (cm/μs)	S	μ (Mb)	Y_0 (Kb)	Γ
Copper	8.93	0.39	1.50	0.46	4.50	2.00
Aluminum	2.71	0.53	1.50	0.25	5.50	1.70
Tungsten	19.23	0.40	1.23	1.54	18.00	1.54
Steel	7.89	0.45	1.50	0.77	6.00	2.02

a 15 Mflop workstation. The simulation shows a depth (46 mm) which is 4% smaller than the experiment (48 mm). The diameter of the hole in Fig. 4b appears to be a constant 12 mm, whereas the SPH result shows some narrowing near the top. The diameter of the SPH hole is near 12 mm through most of its depth. The code shows a crater lip in the steel similar to the experiment. Hohler and Stilp report that no tungsten was found on the sides of the crater hole. This is contrary to the calculation in which the tungsten plated out evenly in the cavity during penetration.

DISCUSSION

A two-dimensional axisymmetric formulation of SPH has been described and three calculations presented. We observe little pathological behavior at the axis but we do see some unphysical motions near the origin in the spherical Noh problem. The formulation presented includes the entire stress tensor, making it applicable to problems where material strength is important. At present the formulation is limited to the use of a Gaussian kernel which is not as efficient as B-splines. Two impact calculations agree very well with experiment but the SPH solution for the Noh problem is not adequate. We hope to see this solution improved by correcting the error at the axis and implementing a tensor viscosity as suggested by Crowley [13]. Run times appear longer than Eulerian, owing mainly to the neighbor searching and particle interactions, but also the Gaussian smoothing function with subsequent evaluation of Bessel functions. SPH has many nice features such as robustness, conceptual simplicity, ease of adding new physics, a natural treatment of voids, accurate tracking of material interfaces and the ability to handle large strains in a pure Lagrangian frame. The method is, however, largely untested for the broad range of problems for which mesh-based techniques have proven useful. Given that three-dimensional calculations are often impractical and that many two-dimensional problems of interest have a symmetry axis, cylindrical SPH should provide the needed test-bed for extensive evaluation of the method. We are encouraged by the results obtained to date.

ACKNOWLEDGMENTS

We thank Dr. Firooz Allahdadi of the Phillips Laboratory and Dr. Per-Anders Persson of New Mexico Tech for their support of this work. We have benefited from discussions with Dr. Stellingwerf and Professor Benz. We thank Pat Crowley for his suggested improvements to the code. Thanks to Ted Carney, Steve Andreson, Scott Maethner, and Dave Amdahl for calculational support.

REFERENCES

1. L. B. Lucy, *Astron. J.* **83**, 1013 (1977).
2. J. J. Monaghan and R. A. Gingold, *J. Comput. Phys.* **52**, 374 (1983).
3. J. J. Monaghan, *SIAM J. Sci. Stat. Comput.* **3**, 422 (1982).
4. J. J. Monaghan, *Comput. Phys. Rev.* **3**, 71 (1985).
5. R. A. Gingold and J. J. Monaghan, *Mon. Not. R. Astron. Soc.* **181**, 375 (1977).
6. R. A. Gingold and J. J. Monaghan, *J. Comput. Phys.* **46**, 429 (1982).
7. W. Benz, *Numerical Modeling of Nonlinear Stellar Pulsation: Problems and Prospects* (Kluwer Academic, Boston, MA, 1990), p. 269.
8. R. H. Durisen, R. A. Gingold, J. E. Tohline, and A. P. Boss, *Ap. J.* **305**, 281 (1986).
9. L. D. Libersky and A. G. Petschek, in *Proceedings, The Next Free Lagrange Conf., Jackson Hole, WY 1990*, edited by H. E. Trease, J. W. Fritts, and W. P. Crowley (Springer-Verlag, New York, 1991).
10. R. A. Stellingwerf, in *Proceedings, The Next Free Lagrange Conf., Jackson Hole, WY 1990*, edited by H. E. Trease, J. W. Fritts, and W. P. Crowley (Springer-Verlag, New York, 1991), p. 395.
11. C. S. Coleman and G. V. Bicknell, *Mon. Not. R. Astron. Soc.* **214**, 337 (1985).
12. W. F. Noh, *J. Comput. Phys.* **72**, 78 (1978).
13. P. Crowley, private communication, Lawerence Livermore National Laboratory, May 1992.
14. A. J. Piekutowski, *Int. J. Impact Eng.* **10**, 453 (1990).
15. V. Hohler and A. J. Stilp, in *Proceedings, 3rd Int. Symp. on Ballistics, 1977*, p. 23.